Carbon Paper as a Promising Free Standing Anode for Sodium Ion Batteries

Journal of The Electrochemical Society, 2020 **167** 160538
1945-7111/2020/167(16)/160538/8/$40.00 © 2020 The Electrochemical Society ("ECS"). Published on behalf of ECS by IOP Publishing Limited

Carbon Paper as a Promising Free Standing Anode for Sodium Ion Batteries

Sadiya Waseem,[1,2,=] C. Nithya,[3,=] Priyanka H. Maheshwari,[1,2,z] and S. R. Dhakate[1]

[1]*CSIR—National Physical Laboratory, Dr. K. S. Krishnan Marg, New Delhi 110012, India*
[2]*Academy of Scientific and Innovative Research (AcSIR), Ghaziabad 201002, India*
[3]*Department of Chemistry, PSGR Krishnammal College for Women, Coimbatore, Tamil Nadu, India*

Porous conducting carbon fiber composite papers have been developed by a two-step process. This involves fabrication of carbon fiber preform followed by composite formation. Different composite papers have been developed by varying the final heat treatment temperature of the composite, viz. 800 °C, 1100 °C, 1400 °C, 1800 °C and 2300 °C. The study gives an insight as to how the structure, porosity, morphology, electrical and mechanical properties of the carbon/carbon composites vary with temperature; and further the effect of these variations on the performance of the composites as anode material for Na-ion batteries. The sample heat-treated to 800 °C showed high reversible capacity of 278 mAh g^{-1} at a current density of 37 mA g^{-1}. Additionally, high columbic efficiency (>99%) and 72% retention of the initial capacity has been demonstrated for 1000 cycles. This exceptional performance is attributed to the small crystallite size, large d-spacing and disordered structure of the sample which favors the insertion/de-insertion of sodium ion into the composite anode. Hence, it seems as a promising anode material for sodium-ion batteries.
 [DOI: 10.1149/1945-7111/abd1f5]

Manuscript submitted September 3, 2020; revised manuscript received November 29, 2020. Published December 21, 2020.

Energy generation and storage are the significant problems concerning the world today.[1] The problem has escalated in the past decade because of high reliance on non-renewable energy resources like oil, coal, etc.[1,2] Such sources of energy are depleting at an exponential rate and their availability is also limited adding to the woes of their soaring market prices. This clearly calls for finding new, renewable, clean, alternative sources for satisfying the energy requirements of the world.[3,4] Global implementation of these renewable sources of energy will require scientific efforts directed towards the production of efficient, and economically viable energy conversion and storage devices.[5–7] Search for such new technologies which can provide and fulfill the mandates of being green, sustainable, recyclable and competent source of energy have been going on tremendously.[7,8] Presently, the technologies known for providing high energy density and durability are mostly batteries,[9,10] fuel cells[11,12] and super capacitors.[13,14] Amongst them the rechargeable battery technology is a preferred choice since it is well established, provides higher output power densities and have low maintenance.[15] Batteries are the most leading contenders in the market, when it comes to efficient energy generation and portable applications. Their versatility have made them cover the entire energy harvesting market single handedly.[15,16] Among the rechargeable batteries, lithium-ion battery (LIB) is the most commonly used energy storage system in portable electronics owing to its high theoretical energy density. The commercial LIBs contain intercalating electrode materials i.e., graphite as the anode and $LiCoO_2$ as the cathode. The theoretical idea related to Sodium ion battery (SIB) was developed parallel to the LIB.[16,17] Sodium is just next to the lithium in the alkaline metallic group, hence they share a lot of common electrochemical and physicochemical properties.[18] SIBs work on the same principle as the LIBs, wherein the charge carrier is Na^+ ion instead of Li^+. The standard electrode potential of Li/Li^+ vs SHE is −3.04 V whereas that of Na/Na^+ is −2.71 V. The highest cell voltage offered by SIBs is 3.6 V which is only slightly lower than 4 V provided by LIBs.[18,19] It is likely that with intelligent research, the present success of LIBs can be a guide to work upon the SIB technology.

Sodium is the fourth abundant element found in the Earth's crust and is almost evenly distributed across all nations, making it easily available and cost effective material for research.[18,19] The ionic radii of sodium is large (1.06 Å) which makes the intercalation difficult, hence affecting its performance.[16–18] However, the abundance of resources and much lower cost have compelled scientists to work towards overcoming the present issues related to SIBs and make them a competent option with respect to LIBs. Room temperature operation, cost effectiveness, safe electrolyte materials, easy handling, and portability have directed the interest of researchers in this technology.[16–18,20] The working of SIB includes extraction of Na^+ ions from cathode and movement towards anode during the process of charging, and during discharge the reverse process occurs with the extraction of Na+ ions from anode and returning back to cathode as being in the initial stage.[18] The main issue of poor diffusion of ions leading to difficulty of intercalation can be tackled by exploring new cathode sources and developing new anodic materials for SIBs.[21] The anode is one of the most critical components since it acts as the host for the sodium ion. It should not only have high storage capacity, but at the same time must be able to maintain its structural integrity over successive cycling. Hence, the investigation for cost effective and efficient anodic material should be widely pursued. In the past, following the trend of LIBs, carbonaceous materials have been used as anodic material for SIBs. Investigations involving use of graphite, expanded graphite, graphene, carbon fibers, carbon black, carbon sheets, porous carbon, CNTs, and other hard carbons as anode have been reported.[19,22,23] The specific capacities were found to be in between 200–500 mAh g^{-1} for these materials with cycle life reported in between 50–200 cycles. The benefits of using carbon materials are their abundance, chemical inertness/safety, variety of forms, stability, low cost and easy availability,[24,25] which can meet the primary requirements of the commercialization of the technology.[18,19,22,23,25]

The present study demonstrates the role of carbon fiber based composite paper as a free standing anode for SIBs, for the first time. Variations in the samples were achieved by varying the final heat treatment temperature (HTT) of the composite and required tests were performed. We herein report exceptionally high cycling rate of 1000 cycles with an output performance of over 200 mAh g^{-1} and 72% capacity retention, attained by the composite sample heat treated to 800 °C. Such remarkable performance can be attributed to the structural stability and short ionic diffusion path for Na^+ ions due to its small crystallite size.

Experimental

Materials and methods.—Carbon paper was developed from polyacrylonitrile (PAN) based T-300 carbon fibers as reinforcement and novolac type phenolic resin as a binder. The first step involves

[=]These authors contributed equally to this work.
[z]E-mail: hedap@nplindia.org

development of carbon fiber preforms in the form of non-woven fiber mat with the help of vacuum infiltration. The method for it has been described in detail elsewhere.[26] These carbon fiber preforms were then impregnated with calculated amount of phenolic resin. The impregnated preforms were compression molded under pressure (100 kg cm^{-2}) and temperature (115 °C). To ensure the proper cross-linking, the molded samples were cured at 150 °C for 1 h. Further, these molded sheets were heat treated to higher temperatures to convert it into all carbon composite and impart the desired strength and electrical conductivity. In the present study, the carbon paper heated to 800 °C, 1100 °C, 1400 °C, 1800 °C and 2300 °C were designated as A1, A2, A3, A4 and A5 respectively. The heat treatment was performed in an inert condition (N_2 atmosphere) with the heating rate of 20 °C per hour upto 1400 °C and thereafter at 150 °C per hour upto 2300 °C.

Characterization techniques.—X-Ray diffraction studies were performed on Rigaku miniflex Powder X-ray Diffractometer using CuKα radiation of 1.5418 Å wavelength. The measurements were carried at the rate of 2° min^{-1} for 2 theta between 0°–40° at 25 °C.

The Raman spectra were obtained on Renishaw Invia Reflex Micro Raman Spectrometer. The samples were excited using 514 nm Argon-ion laser (at 50% power).

Four probe technique was used to determine the electrical conductivity of the samples with the help of Kiethley 2600 System Source Meter. The readings were taken from the different sections of the samples and the reported values are an average along with the standard deviation for 4 data points.

Kerosene density method was used to obtain the apparent porosity of the samples. The readings reported along with standard deviation are an average of 6 repeated experiments.

Three-point bending technique for flexural measurements was performed on the universal Testing Machine (INSTRON, model no. 5967). The measurements were carried out according to ASTM: D 1184-69 standards titled "Flexural strength of Adhesive Bonded Laminated Assemblies." The crosshead speed of 0.5 mm min^{-1} and span length of 20 mm was maintained during testing. The reported data (with the standard deviation) are an average of 5 measurements.

Electro-chemical measurements.—Electrochemical Studies (Galvanostatic and charge-discharge studies) of the carbon paper as anode of SIB was carried out on Neware battery analyzer (China) at room temperature. Circular disc of 18 mm diameter of carbon paper samples were punched and used as it is, as the working electrode (anodes). The cells were fabricated in an argon filled glove box (Vigor, China). Sodium sheets were used as cathode. The electrolyte used was 1 M $NaPF_6$ in 1:1 EC/DEC (EC—ethylene carbonate, DEC—Diethyl carbonate). $NaPF_6$, EC and DEC were purchased from MERCK, Germany.

The cyclic voltammetry (CV) studies were performed on electrochemical workstation (Biologic SAS, France). The scans were carried out at different current rates (0.1 C to 10 C) at the scan rate of 0.1 mV s^{-1}. The voltage cut-off window was fixed between 0.01–1.5 V. Electrochemical impedance spectroscopy (EIS) was performed in the frequency range 100 KHz to 5 MHz at AC voltage amplitude of 5 MV.

Results and Discussion

X–Ray Diffraction analysis.—XRD pattern for the samples A1–A5 has been shown in Fig. 1 and Table I mentions the values of 2θ, calculated d spacing, FWHM (full width at half maximum), and average crystallite size (τ) calculated for all the samples.[27] The d spacing and crystallite size (τ) were obtained from the Bragg's and Scherer's formula respectively according to the following equations.

$$n\lambda = 2d \sin\theta \quad [i]$$

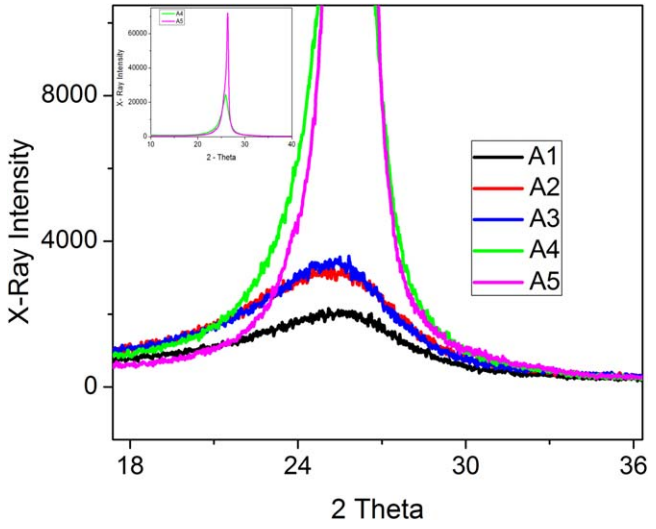

Figure 1. XRD pattern for samples A1–A5.

Where n denotes an integer, λ is the wavelength of X-ray used, d is interplanner spacing and θ denotes diffraction angle.

$$\tau = \frac{k\lambda}{\beta \cos\theta} \quad [ii]$$

Where τ, is average crystallite size, k = 0.9 is the Scherer constant, β represents the FWHM (in radian).[27] The figure clearly shows that with increasing HTT the degree of graphitization attained by the samples increases. Sharp peaks are observed for samples A4 and A5 which indicates that the synthesized composites are highly crystalline in nature. With increasing heat treatment, the d spacing decreases, and correspondingly the crystallite size increases. It should be mentioned that higher d spacing will aid in easy flow of ions across the carbon layers, with the maximum obtained for sample A1 (i.e. 3.51 Å). The increase in crystallite size has been significant from 10.2 Å for A1 to 118.6 Å for A5 which is an increase of more than 900%. However, this increase is very nominal as the composite is heated from 1100 °C to 1400 °C, i.e. from sample A2 to A3. Thus the structure of carbon composites heated to lower temperature is polycrystalline with short range ordering. As will be seen later such structure assists the movement of the ions to and from the composite.

Raman spectroscopy analysis.—Laser Raman spectroscopy is a profound tool to study the graphitic nature of the carbon materials. Raman spectra generally comprises of three major bands, D band, G and G′ band for bulk carbon materials heat treated to elevated temperatures. The D band[28] originates from the structural defects in the samples which can be due to sp^3 carbon, vacancies, hetero atoms etc. The G band relates to presence of graphite like structure as of sp^2 carbon atoms.[28,29] G′ band is the second order harmonic to D band (also known as 2D band), and is a measure of the crystallinity of the material and determines the stacking sequence/arrangement of the hexagonal carbon layers.[28,29] Figure 2 depicts the Raman spectra of synthesized samples A1–A5. The relative intensities of D and G′ bands (I_D/I_G and I_{2D}/I_G calculated by the area under the curve with G band as reference) are shown in inset of Fig. 2. The relative intensity of D bands is highest for sample A1 and decreases with increase in heating temperature suggesting that the disorder in the samples decreases with increasing HTT. I_{2D}/I_G ratio increases slightly for A1–A3 from 0.11 to 0.18, and thereafter increases sharply for A4 and A5. This suggests long range stacking order in samples with heat treatment beyond 1400 °C. The results comply with the observation of the XRD studies.

Table I. D spacing and crystallite size calculated using XRD patterncfor samples A1–A5.

Sample	Heat Treatment (°)	2θ (002) (°)	d_{002}spacing (Å)	FWHM (β) (°)	Crystallite Size (τ) (Å)
A1	800	25.38	3.51	7.89	10.2
A2	1100	25.46	3.49	5.62	14.5
A3	1400	25.48	3.49	5.53	14.7
A4	1800	25.92	3.43	1.76	47.4
A5	2300	26.34	3.38	0.68	118.6

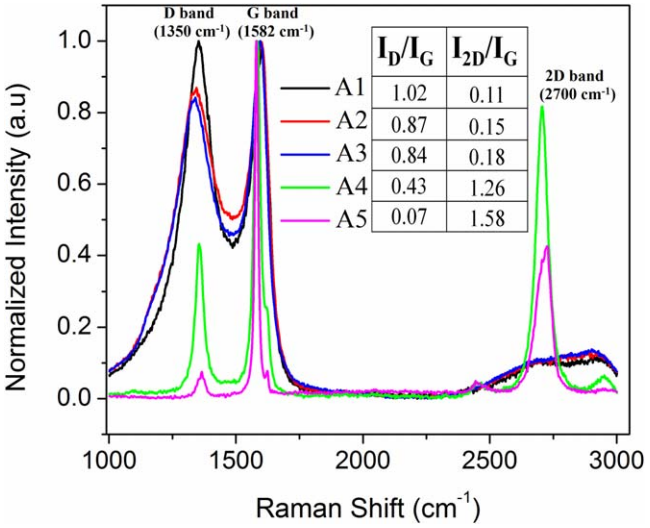

Figure 2. Raman spectra for samples A1–A5.

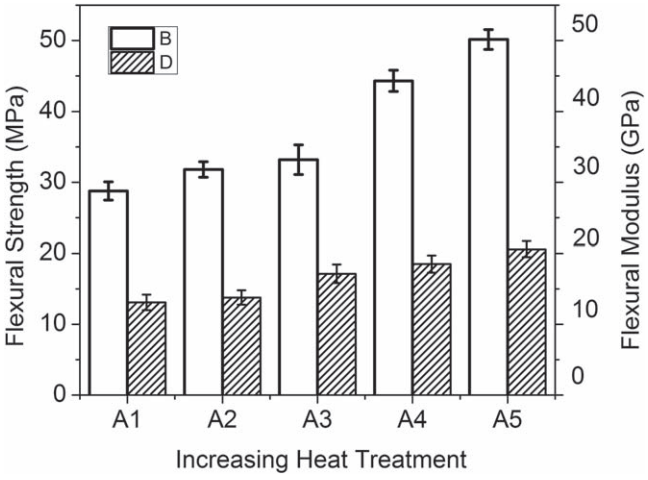

Figure 3. Mechanical properties (strength and modulus) for samples A1–A5.

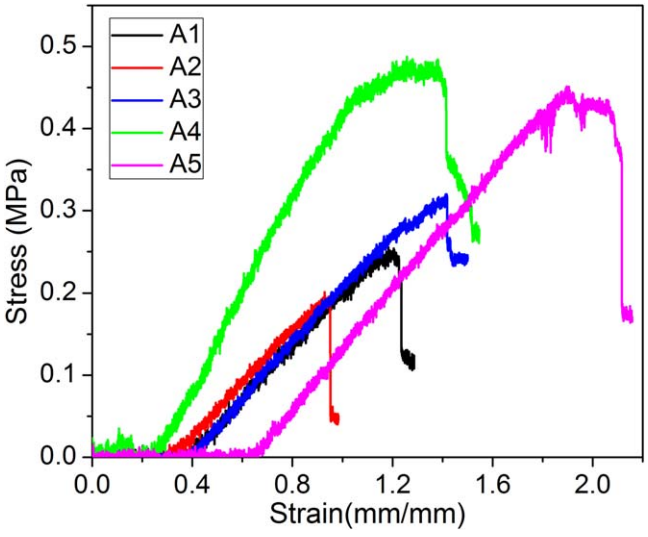

Figure 4. Stress-strain curves for samples A1–A5.

Apparent porosity.—Another important parameter which may affect the performance of battery anode is its porosity. Higher porosity results in an increase in the surface area of the anode in contact with the electrolyte, and may thus affect the performance of the battery.[30] Table II contains the data for porosity and permeability of the samples A1–A5. It can be seen that porosity and permeability both decreases gradually with increasing heat treatment. It is a common phenomenon observed in carbon fiber based composites where the matrix shrinks towards the fiber with increasing HTT, leading to compaction in the structure.[26,31,32] This makes the composites dense and less porous. As shown in the table, there is nearly 12% and 43% reduction in porosity and gas permeability respectively as the pyrolysis temperature of the composite is increased from 800 °C to 2300 °C, owing to the excessive shrinkage of matrix towards the fiber.

Mechanical properties.—The anode of the SIB has been developed by researchers both in powder form and free standing forms like foams, thin films and sheets.[30,33] For a material to act as a free standing battery anode, it should possess enough strength so as to endure the various changes during the cell operation and still retain its structural integrity to ensure long life cycle.[33] As shown in Fig. 3, the flexural strength and modulus values have improved with increase in HTT. Increase in heating temperature, not only leads to an increase in fiber/matrix interaction,[32,34] but at the same time the planes become more and more aligned leading to higher crystallinity

Table II. Porosity and gas permeability of the samples A1–A5.

Sample	Porosity (%)	Gas Permeability (ml × mm × cm^{-2} × mm^{-1} × min^{-1} × Aq^{-1})
A1	83.3 ± 1.2	876.5 ± 6.4
A2	80.1 ± 2.2	788.8 ± 3.2
A3	79.2 ± 1.5	686.3 ± 4.7
A4	77.4 ± 1.1	508.2 ± 5.3
A5	70.8 ± 2.1	495.7 ± 5.1

in the material as seen from above sections (XRD and Raman data). This leads to reduced defects and crack in the samples which could otherwise act as crack initiators,[26,32,35,36] and hence results in improved strength of the composites. The stress-strain curves are plotted for the samples (as shown in Fig. 4). The fracture behavior of the samples resembles that of a typical carbon composites,[26,35,36] wherein samples A1, A2 and A3 shows a brittle nature as visible from the sharp fracture and complete elastic behavior. The samples A4 and A5 however show a plastic region which is an indication of shear failure. Samples A4 and A5 show better stress handling capacity (as is evident from the values of flexural strength) in comparison to A1–A3. Nevertheless, all the samples (A1–A5) have the strength in the required range.

Figure 5 depicts the SEM images of the carbon paper samples. Figure 5 a shows the planer view of the composite, clearly showing the porosity arising majorly due to the fiber arrangement. Further the fractured surfaces of the samples heated to different temperatures show that for samples heated to lower temperatures the matrix structure is smooth and the fracture is quite brittle. However, with increase in pyrolysis temperature the matrix and the fiber/matrix interface graphitizes which is clearly observed by the development of lamellar microstructure in sample A4 which becomes still prominent in A5. Although the fracture is brittle, fiber pullouts are also visible. The development of graphitic structure is responsible for the composite to fail in shear mode rather than pure tensile.[37]

The Fig. 6 shows the electrical conductivity of the samples A1–A5. The conductivity of the samples increases with increasing heat treatment of the composite (the increase being sharp between A2 & A3 and A4 & A5). Overall there is an enhancement of nearly 187% in conductivity with an increase in heat treatment from 800 °C to 2300 °C. The process of heating improves the alignment of the basal planes of the fiber and matrix.[34,38,39] It also graphitizes the fiber/matrix interface (as shown in the SEM images), thus leading to an increase in the electrical conductivity.

Sodium storage capability of carbon papers.—In order to investigate the sodium storage performance of carbon fiber based composites (samples A1–A5) the galvanostatic charge/discharge cycling was carried out at 0.1 C rate (37 mAg^{-1}) within the potential window 0.01 to 1.5 V. The charge/discharge curves of the samples are presented in Fig. 7a. The first cycle charge capacities with samples A1, A2, A3, A4 and A5 as anodes are 278, 46, 117, 0.2 and 7.4 mAh g^{-1}, against the discharge capacities of 295, 165, 215, 10 and 17 mAh g^{-1} respectively. Thus all samples except A1 exhibit

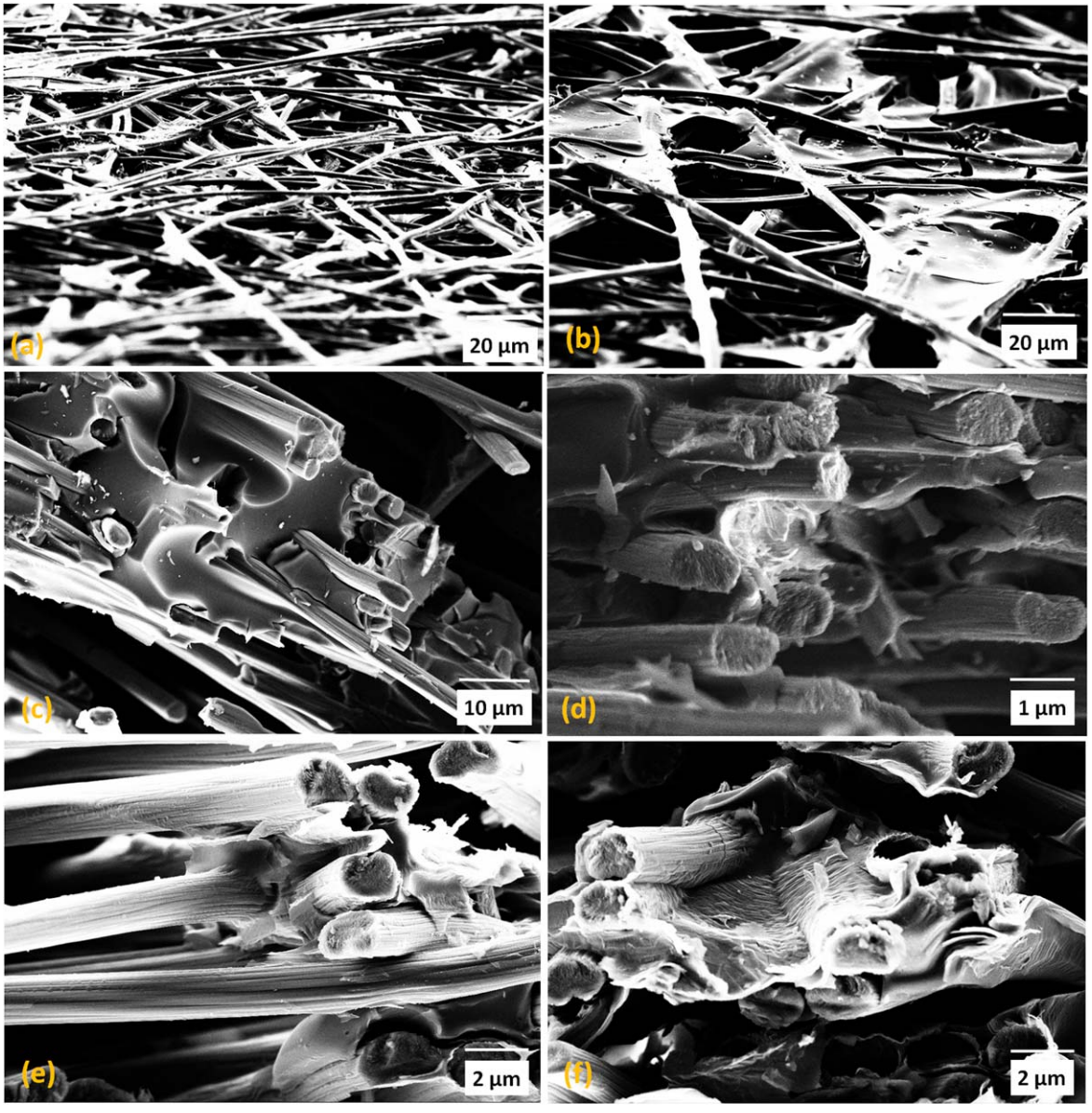

Figure 5. SEM images of carbon paper samples heat treated to (a) and (b) 800 °C, (c) 1100 °C, (d) 1400 °C, (e) 1800 °C, and (f) 2300 °C.

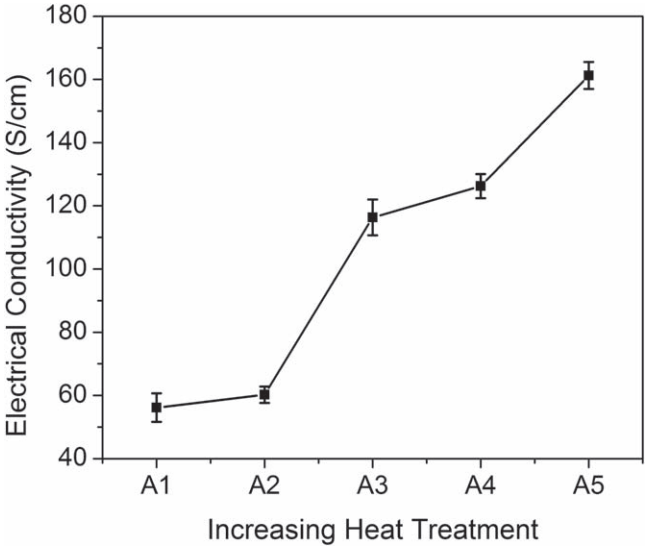

Figure 6. Electrical conductivity (in-plane) for samples A1–A5.

large irreversible capacity in the first cycle, most likely due to the creation of solid electrolyte interface, which consumes large amount of Na^+ ions trapped between the carbon layers. Sample A1 exhibits high capacity in the first cycle as compared to other samples heat treated to high temperatures. This is because with increasing HTT the degree of graphitization increases which in turn leads to long range ordering in the composite samples. This obstructs the fast movement of the Na^+ ions (trapped in the carbon planes, during the charging) at the time of discharge, resulting in lower discharge capacities. Figure 8 compares the ease of movement of Na^+ ion in case of composite with large d spacing and small crystallite size and an opposite scenario for the easy understanding of the concept.

However, the exact trend of decreasing capacities with increasing heat treatment is not followed. Sample A3 exhibits higher discharge capacity as compared to A2. This is probably because there is only a slight increase in the crystallite size from A2 to A3 and the d(002) spacing remains almost the same, on the other hand the increase in electrical conductivity is significant, i.e. nearly 93%. Thus the performance of a battery electrode depends not only on the crystal structure but also on the electrical conductivity, and a balance between the two is a key to achieve the same.

Further, sample A5 shows slightly higher capacity than A4. Although there is a marked change in d(002) spacing and crystallite size on one hand and conductivity on the other, the result suggests that even in case of sample A4, the region difficult for diffusion (as depicted in Fig. 8b.), is not fully utilized, and the increase in conductivity of sample A5 plays its role. Nevertheless, the composites pyrolyzed to high temperatures (beyond 1800 °C) are not fit for battery electrode.

The charge/discharge profiles exhibit the sloping voltage plateaus in the range of 0.4–0.1 V in both charge and discharge curves which confirm the reversible redox behavior of the carbon paper samples. The low performance of samples A2, A3, A4 and A5 may also be ascribed to the sudden volume expansions[40–42] during the intercalation of Na^+ ion due to their increasing stiffness (as shown by the increasing values of flexural modulus) and may result in the generation of cracks in the active particles and pulverization leading to loss of active site for electrochemical reaction. Figure 7b presents the cycling performance of samples A1–A5 for 12 cycles, wherein the performance remains almost the same and only a slight decrease is observed in some cases. Further, sample A1 exhibits excellent cycling performance whereby it delivers a discharge capacity of 278 mAh g^{-1} in the first cycle and retains 72% of the initial capacity at the end of 1000th cycle (Fig. 7c). The columbic efficiency drops initially (due to the formation of SEI) and maintains $>$ 99 % upto 1000 cycles. This excellent performance is attributed to the small crystallite size, large d-spacing (Table I), disordered and porous carbon structure that favors easy insertion and de-insertion of Na^+ ions in between the planes of carbon based composite material. Moreover, the electrical conductivity is sufficient for providing electronic pathways and the porosity of the electrode supports electrolyte penetration during long term cycling, and thus result in increased ionic conductivity and cycling stability.[43] The obtained cycling stability of sample A1 is comparable to that obtained for other hard carbon based anode materials for sodium-ion batteries[44–48] with an additional advantage of being free standing. Inspired by its outstanding performance, the rate capability of sample A1 has been investigated at various current rates (0.1–10 C) and shown in Figs. 7d and 7e. The sample exhibits the reversible capacities of 278, 256, 207, 180, 131, 90 and 52 mAh g^{-1} at the corresponding current rates of 0.1, 0.2, 0.5, 1, 2, 5 and 10 C respectively. It is an encouraging observation that as the current rate is reduced successively to 0.1 C, A1 sample still delivers a discharge capacity of 272 mAh g^{-1} indicating good rate capability, stability and zero memory effect of carbon paper.

Figure 9a depicts the cyclic voltammograms at a scan rate of 0.1 mV s^{-1} for the carbon papers A1–A5. All samples exhibit the same redox behavior except the values of the peak current density and also show the similar behavior in the charge/discharge profiles. The CV curves of A1 sample (Fig. 9b) show the broad anodic and cathodic peak in the range of 0.1–0.4 V, which is a typical behavior of Na^+ intercalation/de-intercalation into graphitic layers.[49] The overlapping of consecutive cycle redox profiles indicates the high reversibility of sodium ion intercalation/de-intercalation into graphitic layers. To understand the electrochemical performance of the samples in a better way, the diffusion behavior of all the samples were analyzed through EIS studies and the corresponding Nyquist plots with fitted equivalent circuit model are shown in Figs. 9c and 9d respectively. All carbon papers exhibit semicircular shape in the high frequency region. Lines inclined at 45° angle appears in the low frequency region. This noticeable low frequency tail is known as Warburg region which is a distinct feature of Na^+ ion diffusion behavior into carbon papers. Even though the carbon papers A2 and A5 show the small R_s and R_{ct} values as compared to other carbon papers, their diffusion characteristics are poor as evident by Warburg region since the linear portions of the curves are deviated from the angle of 45° (the linear region of samples A4 and A5 are also deviated). Sample A1 exhibits a perfect semicircle with the linear region inclined at an angle of 45° indicating the orderly diffusion of Na^+ ions in the composite. To understand it further we have evaluated the diffusion coefficients of all carbon papers through the following equation:

$$D = R^2T^2/2A^2n^4F^4C^2\sigma^2 \qquad [iii]$$

Where, D is the diffusion coefficient, R is real gas constant, T represents absolute temperature in Kelvin, A is the sample's surface area, n stands for the number of electrons transferred during the reaction, F denotes the Faraday constant, C is the concentration of Na^+ ions, and σ is the coefficient of Warburg impedance calculated/obtained from intersection of the straight line on the real axis,[50] equivalent to $(R_s + R_{sf} + R_{ct} - 2\sigma^2C_{dl})$. The calculated values are shown in Table III which clearly shows that samples have diffusion coefficient in the order of 10^{-12} cm^2 s^{-1} which is comparable and superior to that of other carbon based anodes for sodium-ion batteries.[51–53] As apparent by charge/discharge and cyclic voltammetry profiles, A1 show better diffusion property as compared to others. The enhanced diffusion property of A1 is due to small crystallite size, large d-spacing, disordered structure and porosity in the sample which is favorable for sodium ion diffusion into it.

Conclusions

In the present work, for the first time carbon fiber composite paper has been demonstrated as a free standing anode material for

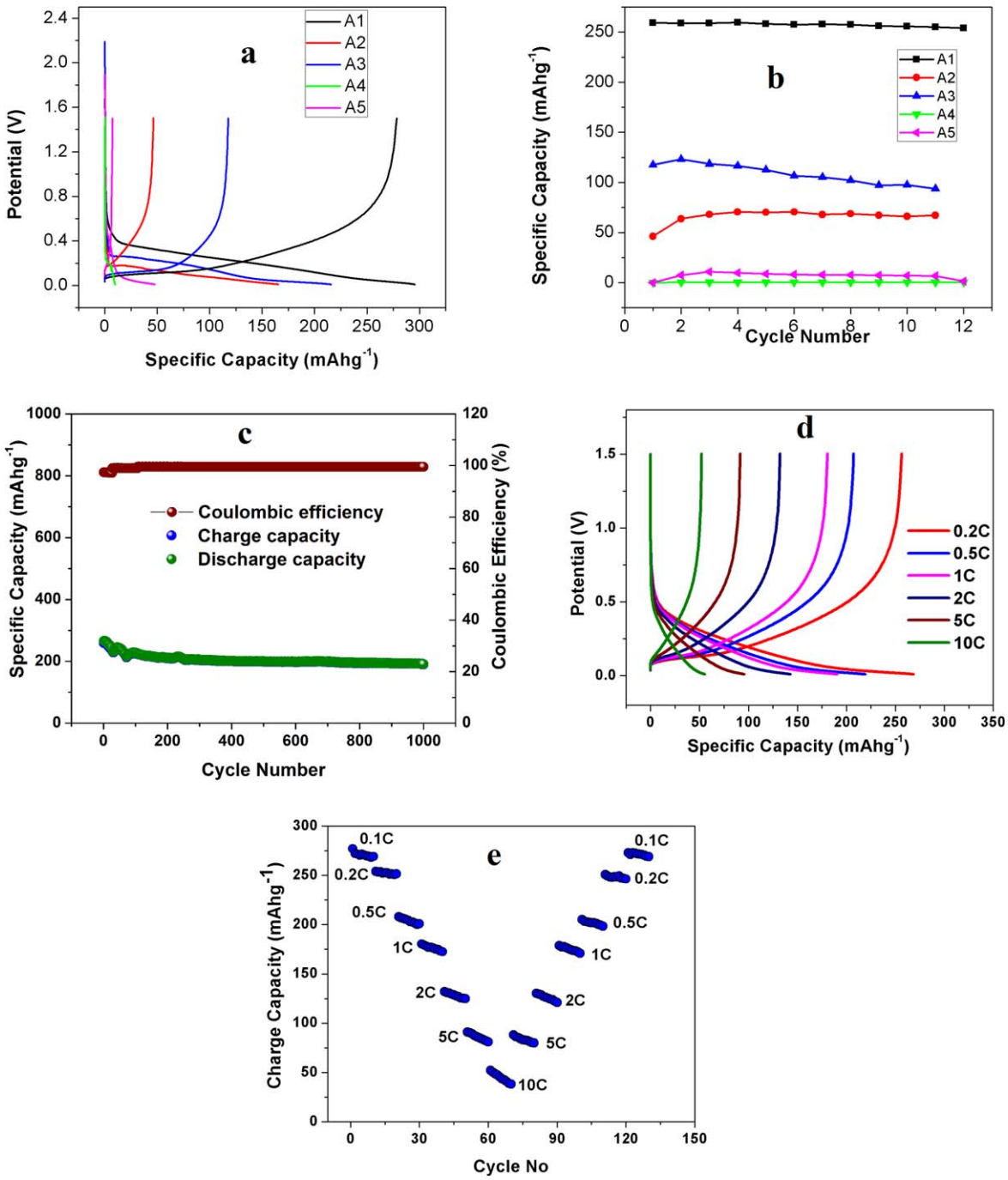

Figure 7. (a) First charge/discharge curves of carbon papers A1–A5 at 0.1 C rate; (b) cycling performance of carbon papers A1–A5 at 0.1 C rate; (c) cycling performance of A1 for 1000 cycles at 0.1 C rate; (d) rate capability curves of A1 at different current rates; (e) rate capability of A1 over 150 cycles at different current rates.

sodium ion batteries. Variations in the properties of the carbon papers have been introduced by varying the final temperature of heat treatment during the process of composite formation. The crystallite size increases gradually as the temperature is raised from 800 °C to 1400 °C, and thereafter the increase is significant, due to long range ordering and graphitization of the composite. The increased graphitic nature is responsible for the samples (A4 and A5) to fail in shear mode. The electrical conductivity observes a sharp hike between 1100 °C to 1400 °C and 1800 °C to 2300 °C. The overall performance of the samples as anode for SIB depends on the balance between the different properties. The sample heat treated to 800 °C showed high reversible capacity (278 mAh g^{-1}) and exceptional durability with a capacity retention of 72% after 1000 cycles. The outstanding performance can be associated with the high lattice spacing (3.51 Å) and small crystallite size (10.2 Å) which aids in easy to and fro motion of sodium ions across the electrode. The columbic efficiency of this material is above 99 % which also suggests that it is a promising material to be used as as anode of sodium ion battery applications.

Acknowledgments

The authors are grateful to the CSIR for providing funds under the CSIR NMITLI (New Millennium Indian Technology Leadership Initiative) project 'Demonstration & Validation of 5 kW HT PEMFC based combined cooling and power system. Thanks are also due to

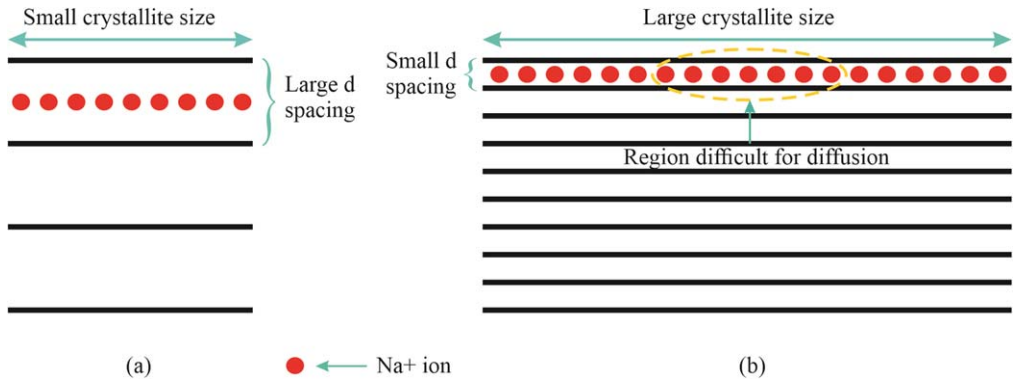

Figure 8. Schematic of the movement of sodium ion in C/C composite system heat treated to (a) lower temperature and (b) higher temperature.

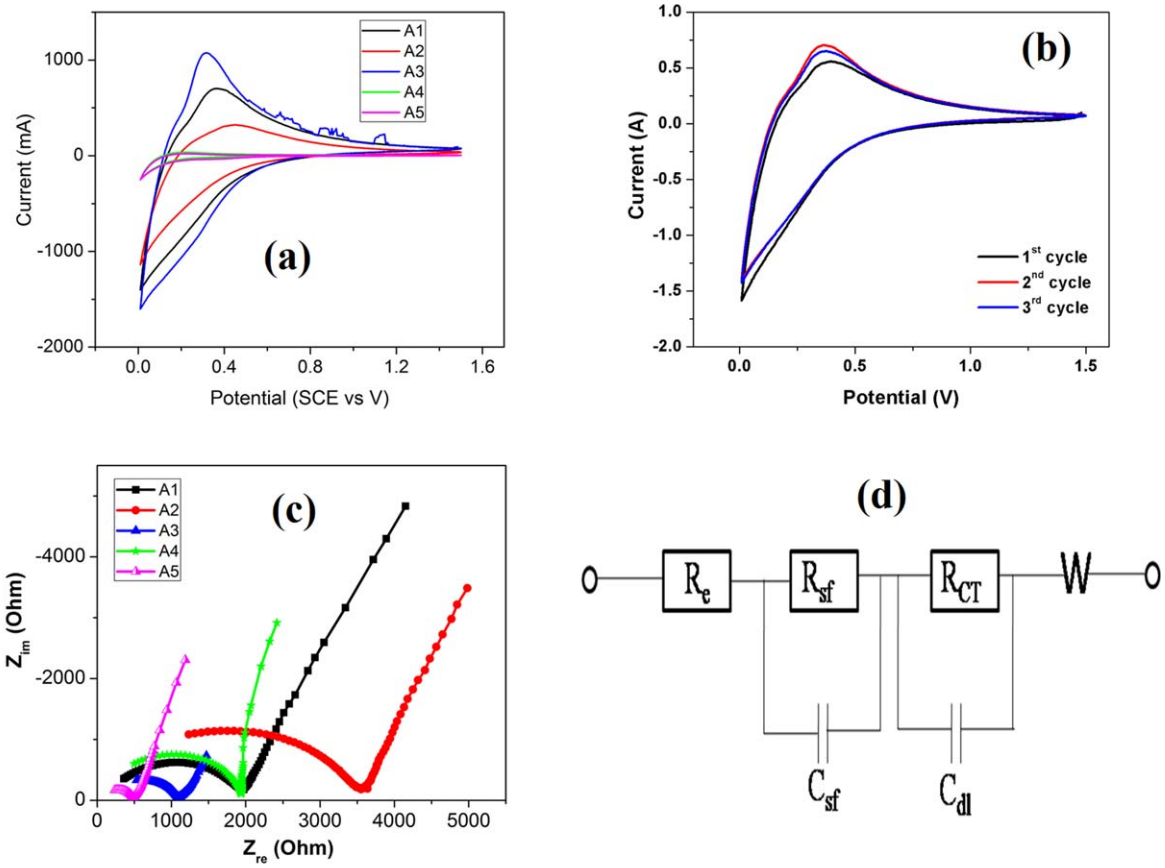

Figure 9. (a) Cyclic voltammograms of A1–A5 (scan rate 0.1 mV s^{-1}); (b) cyclic voltammograms of sample A1 at the scan rate of 0.1 mV s^{-1}; (c) Nyquist plots for samples A1–A5; (d) equivalent circuit model for Nyquist plots of samples A1–A5.

Table III. EIS parameters of carbon papers A1–A5.

Sample	R_s (Ω)	R_{ct} (Ω)	C_{dl}(mF)	Diffusion coefficient (cm^2 s^{-1})
A1	97	1887	60.2	2.62×10^{-12}
A2	125	360	55.8	9.91×10^{-12}
A3	298	1647	32.8	1.45×10^{-12}
A4	742	2803	47.6	1.13×10^{-12}
A5	402	695	38.2	2.98×10^{-12}

Shaveta Sharma for the flexural experiments, Naval Kishor for the XRD analysis. For the inspire fellowship, Two authors, Sadiya Waseem and C. Nithya would like to thank and acknowledge Department of Science and Technology (DST, India) for Inspire fellowship and DST-Women Scientist Award (SR/WOS-A/CS-20/2017) respectively.

ORCID

Priyanka H. Maheshwari https://orcid.org/0000-0002-7518-0283

References

1. E. Haghi, M. Fowler, and K. Raahemifar, *Int. J. Hydrogen Energy*, **44**, 9643 (2019).
2. D. Helm, *Burn out: Theendgame for fossil fuels.* (Yale University Press., New Haven, Connecticut) (2017).
3. C. A. Simon, *Alternative Energy: Political, Economic, and Social Feasibility* (Rowman & Littlefield Publishers) (2020).
4. L. Gubacheva, I. Makarova, S. Andreev, A. Andreev, and D. Shevchenko, *Journal of Physics: Conference Series*, 012094 (2019).
5. S. Skinner, *Energy Storage and Conversion Materials* (Royal Society of Chemistry, United Kingdom) 5 (2019).
6. S. Yun, Y. Zhang, Q. Xu, J. Liu, and Y. Qin, *Nano Energy*, **60**, 600 (2019).
7. S. Iqbal, H. Khatoon, A. H. Pandit, and S. Ahmad, *Materials Science for Energy Technologies*, **2**, 417 (2019).
8. M. Khalil, M. A. Berawi, R. Heryanto, and A. Rizalie, *Renew. Sustain. Energy Rev.*, **105**, 323 (2019).
9. M. S. Whittingham, R. F. Savinell, and T. Zawodzinski, *Introduction: Batteries and Fuel Cells* (ACS Publications, Washington DC) (2004).
10. G. Smith, *Storage Batteries: Including Operation, Charging, Maintenance and Repair* (Pitman Advanced Pub. Program, Boston) (1980).
11. F. Barbir, *Fuel Cell Technology* (Springer, Berlin) p. 27 (2006).
12. X. Zhang and Z. Shen, *Fuel*, **81**, 2199 (2002).
13. L. L. Zhang and X. Zhao, *Chem. Soc. Rev.*, **38**, 2520 (2009).
14. E. Frackowiak, *Phys. Chem. Chem. Phys.*, **9**, 1774 (2007).
15. G. Pistoia, *Lithium-ion Batteries: Newness, Advances and Applications* (Elsevier, Amsterdam, United Kingdom) (2013).
16. M. D. Slater, D. Kim, E. Lee, and C. S. Johnson, *Adv. Funct. Mater.*, **23**, 947 (2013).
17. N. Yabuuchi, K. Kubota, M. Dahbi, and S. Komaba, *Chem. Rev.*, **114**, 11636 (2014).
18. J.-Y. Hwang, S.-T. Myung, and Y.-K. Sun, *Chem. Soc. Rev.*, **46**, 3529 (2017).
19. S. W. Kim, D. H. Seo, X. Ma, G. Ceder, and K. Kang, *Adv. Energy Mater.*, **2**, 710 (2012).
20. H. Pan, Y.-S. Hu, and L. Chen, *Energy & Environmental Science*, **6**, 2338 (2013).
21. A. Ponrouch, A. Goñi, and M. R. Palacín, *Electrochem. Commun.*, **27**, 85 (2013).
22. R. Alcántara, J. M. Jiménez-Mateos, P. Lavela, and J. L. Tirado, *Electrochem. Commun.*, **3**, 639 (2001).
23. Y. Wen, K. He, Y. Zhu, F. Han, Y. Xu, I. Matsuda, Y. Ishii, J. Cumings, and C. Wang, *Nat. Commun.*, **5**, 4033 (2014).
24. X. Zhou and Y. G. Guo, *Chem. Electro. Chem*, **1**, 83 (2014).
25. S. Wenzel, T. Hara, J. Janek, and P. Adelhelm, *Energy & Environmental Science*, **4**, 3342 (2011).
26. S. Waseem, P. H. Maheshwari, S. Abinaya, A. K. Sahu, A. Saini, and S. R. Dhakate, *Int. J. Energy Res.*, **43**, 2897 (2019).
27. N. Iwashita, C. R. Park, H. Fujimoto, M. Shiraishi, and M. J. C. Inagaki, *Carbon*, **42**, 701 (2004).
28. A. Cuesta, P. Dhamelincourt, J. Laureyns, A. Martinez-Alonso, and J. D. J. C. Tascón, *Carbon*, **32**, 1523 (1994).
29. A. C. J. S. S. C. Ferrari, *Solid State Communications*, **143**, 47 (2007).
30. C. Nithya and S. J. Gopukumar, *Wiley Interdisciplinary Reviews: Energy and Environment*, **4**, 253 (2015).
31. P. H. Maheshwari, *Materials Science for Energy Technologies*, **2**, 490 (2019).
32. R. Mathur, P. H. Maheshwari, T. Dhami, and R. Tandon, *Electrochim. Acta*, **52**, 4809 (2007).
33. H. Hou, X. Qiu, W. Wei, Y. Zhang, and X. J. Ji, *Advancedenergy materials*, **7**, 1602898 1602898 (2017).
34. K. Lee and Z. Y. Chen, *Materials chemistry and physics*, **82**, 428 (2003).
35. K. Goto, H. Hatta, M. Oe, and T. J. Koizumi, *Journal of the American Ceramic Society*, **86**, 2129 (2003).
36. G. Davies and X. J. Zhang, *International Journal of Impact Engineering*, **16**, 149 (1995).
37. W. Avery and C. Herakovich, *Journal of Applied Mechanics*, **53**, 751 (1986).
38. J. Don and C. P. Ju, *Materials Science and Engineering: A*, **124**, 259 (1990).
39. C. P. Ju and N. Murdie, *Materials chemistry and physics*, **34**, 244 (1993).
40. Y. Cao, L. Xiao, M. L. Sushko, W. Wang, B. Schwenzer, J. Xiao, Z. Nie, L. V. Saraf, Z. Yang, and J. J. N. L. Liu, *Nano letters*, **12**, 3783 (2012).
41. B. Jache and P. J. A. C. I. E. Adelhelm, *Angewandte Chemie International Edition*, **53**, 10169 (2014).
42. L. Qie, W. Chen, H. Xu, X. Xiong, Y. Jiang, F. Zou, X. Hu, Y. Xin, Z. Zhang, and Y. J. E. Huang, *Energy& Environmental Science*, **6**, 2497 (2013).
43. Z. Li, G. Li, J. Ouyang, B. He, L. Chen, W. Wang, M. Zhou, W. Xu, Y. Zhang, and Z. J. C. Hou, *Chemistry Select*, **4**, 5768 (2019).
44. X. Chen, Y. Zheng, W. Liu, C. Zhang, S. Li, and J. J. N. Li, *Nanoscale*, **11**, 2219622196 (2019).
45. D.-Y. Kim, D.-H. Kim, S.-H. Kim, E.-K. Lee, S.-K. Park, J.-W. Lee, Y.-S. Yun, S.-Y. Choi, and J. J. N. Kang, *Nanomaterials*, **9**, 793 (2019).
46. A. Kamiyama, K. Kubota, T. Nakano, S. Fujimura, S. Shiraishi, H. Tsukada, and S. J. Komaba, *ACS Applied Energy Materials*, **3**, 135 (2019).
47. X. Dou, I. Hasa, D. Saurel, C. Vaalma, L. Wu, D. Buchholz, D. Bresser, S. Komaba, and S. J. M. T. Passerini, *Materials Today*, **23**, 87-104 (2019).
48. M. Anji Reddy, M. Helen, A. Groß, M. Fichtner, and H. J. Euchner, *ACS Energy Letters*, **3**, 2851 (2018).
49. Y. Jin, S. Sun, M. Ou, Y. Liu, C. Fan, X. Sun, J. Peng, Y. Li, Y. Qiu, and P. J. Wei, *ACS Applied Energy Materials*, **1**, 2295 (2018).
50. M. Shi, Z. Chen, J. J. C. Sun, and C. Research, *Cement and Concrete Research*, **29**, 1111 (1999).
51. X. Li, X. Zeng, T. Ren, J. Zhao, Z. Zhu, S. Sun, and Y. J. Zhang, *Journal of Alloys and Compounds*, **787**, 229 (2019).
52. Z. L. Xu, J. Park, G. Yoon, H. Kim, and K. J. S. M. Kang, *Small Methods*, **3**, 1800227 (2019).
53. B. Cao, H. Liu, B. Xu, Y. Lei, X. Chen, and H. J. J. O. M. C. A. Song, *Journal of Materials Chemistry A*, **4**, 6472 (2016).